Contribution from the Chemistry Department,
University of Virginia, Charlottesville, Virginia 22901

Measurement and Analysis of Circular Dichroism in the 4f–4f Transitions of Ho^{3+} in $Na_3[Ho(C_4H_4O_5)_3]\cdot 2NaClO_4\cdot 6H_2O$

Diane M. Moran and F. S. Richardson*

Received August 6, 1991

Optical absorption and circular dichroism (CD) measurements are reported for Ho^{3+} in single crystals of $Na_3[Ho(ODA)_3]\cdot 2NaClO_4\cdot 6H_2O$ (where ODA denotes a terdentate *oxydiacetate* ligand). These measurements span the 15 000–27 000-cm^{-1} spectral region, and they encompass the following *J*-multiplet-to-*J*-multiplet transition manifolds of $Ho^{3+}(4f^{10})$: $^5I_8 \rightarrow {}^5F_5$, $^5S_2$, $^5F_4$, $^5F_3$, $^5F_2$, $^3K_8(2)$, $^5G_6$, $^5F_1$, $^5G_5$, $^5G_4$, and $^3K_7(2)$, where the multiplets are labeled according to their principal *SLJ* parentage in the $4f^{10}$ electronic configuration of Ho^{3+}. Observed CD and absorption line intensities are used to determine the electronic rotatory strengths and absorption dissymmetry factors for 24 transitions between crystal-field (Stark) levels. The empirically determined rotatory strength and absorption dissymmetry data are compared to results obtained from direct calculations of the chiroptical properties of 4f–4f transitions in $Na_3[Ho(ODA)_3]\cdot 2NaClO_4\cdot 6H_2O$. These calculations are based on a model used previously to rationalize the $4f^{10}$ electronic state structure and 4f–4f transition intensities of Ho^{3+} in this system. The empirical data combined with the model calculations provide insights regarding (1) the extent of crystal-field-induced *J*-multiplet mixings and (2) the distribution of rotatory strength both *within* and *among* different multiplet-to-multiplet transition manifolds. Results from the model calculations are also used to generate simulated CD spectra that can be compared to experimental spectra throughout congested transition regions. In general, the model calculations provide a satisfactory basis for assigning and interpreting the observed CD and absorption spectra, and they give essential assistance for estimating the relative electric dipole versus magnetic dipole contributions to transition rotatory strengths.

Introduction

In two previous papers[1,2] we reported polarized and unpolarized absorption spectra, crystal-field energy-level analyses, and transition line-strength analyses for Ho^{3+} in single crystals of $Na_3[Ho(ODA)_3]\cdot 2NaClO_4\cdot 6H_2O$ (where ODA denotes a terdentate *oxydiacetate* ligand, $C_4H_4O_5^{2-} \equiv {}^-OOCCH_2OCH_2COO^-$). The absorption spectra spanned the 8000–37000-cm^{-1} region, and 105 crystal-field energy levels were located and assigned from the absorption data. Line strengths were determined for 42 transitions observed in the unpolarized *axial* absorption spectra and for 19 transitions observed in the π-polarized *orthoaxial* absorption spectra. The energy-level data was analyzed in terms of a model Hamiltonian for the $4f^{10}$ electronic structure of Ho^{3+} in a crystal field of trigonal dihedral (D_3) symmetry,[1] and a parametrized form of the Hamiltonian produced calculated-to-empirical energy-level fits with an overall rms deviation of 9.1 cm^{-1}. The eigenvectors of this parametrized Hamiltonian were then used in subsequent transition line-strength analyses,[2] which were based on an intensity model proposed by Reid and Richardson[3] for transitions between crystal-field levels in lanthanide systems. In this intensity model, electric dipole contributions to transition line strengths may be parametrized, and the relevant parameters can be evaluated from fits of calculated-to-empirical line-strength data. Parametric fits of the line-strength data for Ho^{3+} in $Na_3[Ho(ODA)_3]\cdot 2NaClO_4\cdot 6H_2O$ were remarkably successful, and model calculations and simulations of both polarized and unpolarized absorption spectra gave results in excellent agreement with experiment.[2]

The energy-level and intensity analyses reported in our earlier work on $Na_3[Ho(ODA)_3]\cdot 2NaClO_4\cdot 6H_2O$ (abbreviated hereafter as HoODA) suggest that the model Hamiltonian and intensity parameters derived from those analyses might be satisfactory for analyzing the 4f–4f chiroptical properties of HoODA. Chiroptical properties of lanthanide systems are extremely sensitive to the details of $4f^N$ electronic state structure and 4f–4f transition mechanisms, and their analysis and interpretation make stringent demands on theoretical models of $4f^N$ state structure and 4f–4f optical processes.[4-6] Single crystals of $Na_3[Ho(ODA)_3]\cdot 2NaClO_4\cdot 6H_2O$ have the space group $R32$, and they grow (spontaneously) in two enantiomorphic forms which differ with respect to the absolute configuration of their constituent $Ho(ODA)_3^{3-}$ complexes *and* the chiral (left-handed vs right-handed) arrangement of these complexes about the trigonal axis of the crystal. These crystals exhibit *natural* optical rotatory properties[7] and circular dichroism,[8] and their circular dichroism (CD) spectra exhibit large variations in the signs and intensities of CD lines observed within different transition regions.

In the present paper, we report CD measurements carried out on single crystals of HoODA at temperatures between 10 and 295 K. These measurements span the 15 000–27 000-cm^{-1} spectral region, and they encompass the following multiplet-to-multiplet transition manifolds of $Ho^{3+}(4f^{10})$, $^5I_8 \rightarrow {}^5F_5$, $^5S_2$, $^5F_4$, $^5F_3$, $^5F_2$, $^3K_8(2)$, $^5G_6$, $^5F_1$, $^5G_5$, $^5G_4$, and $^3K_7(2)$, where multiplets are labeled according to their principal *SLJ* parentage.[1] Locations and assignments of crystal-field levels split out of these multiplets are given in Table II of ref 1. The excited multiplets contain a total of 69 crystal-field levels, 17 of which have A_1 symmetry, 16 of which have A_2 symmetry, and 36 of which have E symmetry in the D_3 point group. Only two crystal-field levels of the $^5I_8$ (ground) multiplet are thermally populated at 10 K, the ground level (E symmetry) and the first excited level (A_1 symmetry) located 14 cm^{-1} above the ground. In *axial* CD/absorption experiments (light propagation along the trigonal axis of the crystal), *all* $E \rightarrow A_1$, A_2, and E crystal-field transitions are electric *and* magnetic dipole allowed by D_3 symmetry selection rules,[1] whereas for transitions originating from an A_1 crystal-field level, only those terminating on an E level are electric and magnetic dipole allowed. Therefore, in *axial* CD/absorption experiments carried out over the 15 000–27 000-cm^{-1} spectral range (for HoODA at 10 K), one may anticipate the possible appearance of 69 CD-active transitions originating from the ground crystal-field level of $^5I_8$ and 36 CD-active transitions originating from the first excited level of $^5I_8$.

The signs and intensities of CD lines are determined by transition rotatory strengths, which, to lowest order, are defined in terms of scalar products between electric and magnetic dipole transition vectors.[4] Therefore, according to this lowest-order representation of rotatory strengths, a transition between two states *a* and *b* is CD-active only if the pseudoscalar quantity, $|\mu_{ab}||\mathbf{m}_{ab}|\cos$

(1) Moran, D. M.; De Piante, A.; Richardson, F. S. *Phys. Rev. B* **1990**, *42*, 3317.
(2) Moran, D. M.; Richardson, F. S. *Phys. Rev. B* **1990**, *42*, 3331.
(3) (a) Reid, M. F.; Richardson, F. S. *J. Chem. Phys.* **1983**, *79*, 5735. (b) Reid, M. F.; Richardson, F. S. *J. Phys. Chem.* **1984**, *88*, 3579.
(4) Richardson, F. S. *J. Less-Common Met.* **1989**, *149*, 161.
(5) May, P. S.; Reid, M. F.; Richardson, F. S. *Mol. Phys.* **1987**, *62*, 341.
(6) Berry, M. T.; Schwieters, C.; Richardson, F. S. *Chem. Phys.* **1988**, *122*, 125.
(7) Norden, B.; Grenthe, I. *Acta Chem. Scand.* **1972**, *26*, 407.
(8) Moran, D. M.; De Piante, A.; Richardson, F. S. *J. Less-Common Met.* **1989**, *148*, 297.

0020-1669/92/1331-0813$03.00/0 © 1992 American Chemical Society

θ, is nonzero (where μ_{ab} and $\mathbf{m}_{ab}$ denote electric and magnetic dipole transition vectors, respectively, and θ denotes the angle between these vectors). Successful calculations of transition rotatory strengths (and CD line intensities) require that both the magnitudes and relative orientations of the electric *and* magnetic dipole transition vectors be known (or calculable).[4-6] Such calculations for lanthanide 4f–4f transitions present a formidable challenge, but some success has been achieved in previous work on the Sm^{3+} and Eu^{3+} homologues of HoODA.[5,6] In the present paper, we report calculations of transition rotatory strengths and CD spectra for HoODA and then compare the results of these calculations with experimental data. The calculations are based on the parametrized energy-level and transition-intensity models described previously for HoODA,[1,2] and they are similar in execution to those reported in our earlier work on SmODA[5] and EuODA.[6]

Among the 105 CD-active transitions predicted to occur over the spectral range encompassed by our experimental measurements (vide supra), only 24 exhibit CD lines that are sufficiently intense *and* well-resolved to permit quantitative evaluation of rotatory strengths. Therefore, comparisons between calculations and experiment are based in large part on comparisons of experimental spectra with simulated spectra (generated from calculated rotatory strengths).

Experimental Section

Single crystals of $Na_3[Ho(ODA)_3]\cdot 2NaClO_4\cdot 6H_2O$ were grown from aqueous solution following the methods of Albertsson.[9] All of the CD/absorption spectra presented in this paper were obtained on crystals of like enantiomorphic form. Circular dichroism and absorption spectra were measured *simultaneously* using a CD/absorption spectrophotometer designed and constructed at the University of Virginia. Spectra were recorded over the 370–670-nm wavelength range at a constant spectral resolution of ≈0.1 nm. All measurements were performed with the unique (optic) axis of the crystal sample aligned parallel to the direction of light propagation. Variable-temperature measurements between 10 and 295 K were carried out with the crystal sample mounted at the cold station in the sample compartment of a CTI-Cryogenics closed-cycle helium refrigerator and cryostat. The crystal was mounted on a one-piece copper mount using Crycon grease and indium foil, and the copper mount was attached to the cold head of the refrigerator, with strips of indium providing a thermally conductive interface. Cold-head temperature was controlled using a Lake Shore Cryotronics, Inc., temperature controller (Model DRC-70), and it could be varied between approximately 10 K and room temperature.

Damp Whatman glass–microfiber filter paper was used to polish crystals to a thickness and shape suitable for optical measurements. All of the data reported in this paper were obtained from measurements on a crystal of 0.33 mm thickness (optical pathlength).

Calculations and Data Analysis

All of the features observed in the CD/absorption spectra measured in this study can be assigned to electronic origin (zero-phonon) transitions between crystal-field levels of the Ho^{3+} $4f^{10}$ electronic configuration in $Na_3[Ho(ODA)_3]\cdot 2NaClO_4\cdot 6H_2O$. In previous work,[1,2] we have characterized most of these transitions with respect to their symmetry properties (assuming a crystal field of D_3 point-group symmetry) *and* the J-multiplet parentages of their connecting crystal-field levels. We have also previously reported absorption line-strength data and intensity calculations for the transition regions of interest in the present study.[2] The calculations, methods of data analysis, and results presented in refs 1 and 2 are highly relevant to the present study, and the reader is referred to those references for details. Here we shall focus our attention on the analysis of circular dichroic properties.

The circular dichroism associated with a particular electronic transition, A → B, may be expressed as

$$\Delta\epsilon(\bar{\nu}) = \epsilon_L(\bar{\nu}) - \epsilon_R(\bar{\nu}) = 4.354 \times 10^{38}\bar{\chi}[X_A(T)]g_A^{-1}R_{AB}\bar{\nu}\rho_{AB}(\bar{\nu}) \quad (1)$$

where $\epsilon_L(\bar{\nu})$ and $\epsilon_R(\bar{\nu})$ are molar decadic absorption coefficients for left (L) and right (R) circularly polarized light of wavenumber $\bar{\nu}$, $\bar{\chi}$ is a factor dependent on the refractivity of the bulk sample medium (under the specified sample conditions), $X_A(T)$ is the fractional thermal (Boltzmann) population of level A at the sample temperature (T), g_A is the electronic degeneracy of level A, $\rho_{AB}(\bar{\nu})$ is a unit-normalized line-shape function centered at the A → B transition frequency $\bar{\nu}_{AB}$ ($\bar{\nu}$ is expressed in cm^{-1}), and R_{AB} is the *rotatory strength* of the A → B transition (expressed in the cgs units, $esu^2\ cm^2$). The *integrated intensity* of the A → B CD line is related to rotatory strength according to

$$R_{AB}(esu^2cm^2) = 2.297 \times 10^{-39}\left[\frac{g_A}{\bar{\chi}X_A}\right]\int_{A\rightarrow B}\frac{\Delta\epsilon(\bar{\nu})}{\bar{\nu}}\,d\bar{\nu} \quad (2)$$

where the integration is over the A → B transition line width.

The electronic transitions of interest in this study occur predominantly via electric and magnetic dipole mechanisms, and to a very good approximation their rotatory strengths may be expressed entirely in terms of electric and magnetic dipole transition moments.[4,10,11] For transitions observed in the uniaxial single-crystal CD/absorption spectra measured in this study, the rotatory strengths may be expressed as

$$R_{AB} = \tfrac{3}{2}\ \mathrm{Im}\sum_a\sum_b\sum_q\langle A_a|\mu_q|B_b\rangle\langle A_a|m_q|B_b\rangle^* q^2 \quad (3)$$

where Im signifies the imaginary part of (the quantities that follow); a and b label degenerate components of levels A and B, respectively; and μ_q and m_q are the qth components of the electric dipole and magnetic dipole moment operators, expressed in a spherical coordinate basis (q = 0, ±1) with q = 0 defined to be parallel to the direction of light propagation. (In HoODA crystals, the q = 0 direction is also parallel to the trigonal symmetry axis of the $Ho(ODA)_3^{3-}$ complexes.)

Transition rotatory strengths may be determined from CD intensity data according to eq 2 if the degeneracy and fractional thermal population of level A are known, if the $\bar{\chi}$ factor can be evaluated, *and* if the CD lines of interest are sufficiently well-resolved to permit their separate integrations. To a good approximation, the $\bar{\chi}$ factor may be calculated from refractive index data according to: $\bar{\chi} = (n_\alpha^2 + 2)/3$, where n_α denotes the refractive index measured along the optic axis of the crystal.

Direct calculation of transition rotatory strengths from eq 3 requires calculations of electric and magnetic dipole transition moments. The strategy and methods used to perform these calculations have been described in our previous work on lanthanide optical activity.[4-6] Following that work, the axial rotatory strength defined by eq 3 may be reexpressed as

$$R_{AB} = \tfrac{3}{2}e\ \mathrm{Im}\left[\sum_{\lambda,t,p}A_{tp}^{\lambda}\sum_{l,q}\langle\lambda l,\ 1-q|tp\rangle q^2\sum_{a,b}\langle\Psi_{A_a}|U_t^{\lambda}|\Psi_{B_b}\rangle\langle\Psi_{A_a}|m_q|\Psi_{B_b}\rangle^*\right] \quad (4)$$

where e is the elementary charge, the A_{tp}^{λ} are electric dipole intensity parameters (as defined by Reid and Richardson),[3] U_t^{λ} is the tth component of an intraconfigurational unit-tensor operator of rank λ, and Ψ_{A_a} and Ψ_{B_b} are crystal-field state vectors (*excluding* radial parts) expressed in a $|(4f^N)SLJM_J\rangle$ basis. For HoODA, the state vectors and intensity parameters needed to evaluate eq 4 are available from the work reported in refs 1 and 2. The state vectors are eigenvectors of the parametrized model Hamiltonian described in ref 1, and the intensity parameters may be taken directly from the analysis described in ref 2. Both the state vectors and the intensity parameters reflect D_3 symmetry at the Ho^{3+} sites in HoODA.

An expansion of eq 4 in the intermediate-coupling basis for the Ψ_{A_a} and Ψ_{B_b} state vectors is given in the Appendix of ref 5. In this expanded form of eq 4, the only nonvanishing terms are those that satisfy the following selection rules: ΔJ = 0, ±1, and ΔM_J = ±1. In the absence of crystal-field-induced J-multiplet mixing, these selection rules would be satisfied within only *two* of the 11 multiplet-to-multiplet transition manifolds examined in this study, $^5I_8 \rightarrow {}^3K_8(2)$ and $^5I_8 \rightarrow {}^3K_7(2)$. Circular dichroism observed in the other nine multiplet-to-multiplet transition manifolds has *essential* dependence on crystal-field-induced J-multiplet mixing, and the observed CD line intensities provide a sensitive diagnostic probe of this mixing.

Rotatory strengths calculated from eq 4 may be inserted into eq 1 along with suitable line-shape functions and values for $\bar{\chi}$, X_A, and g_A, and CD spectra may then be calculated (or simulated) by evaluating the following expression over the wavenumber range of interest:

$$\Delta\epsilon(\bar{\nu}) = 4.354 \times 10^{38}\bar{\nu}\sum_{A\rightarrow B}\bar{\chi}X_A g_A^{-1}R_{AB}\rho_{AB}(\bar{\nu}) \quad (5)$$

where the summation is over all transitions falling within the specified spectral region and the wavelength dependence of $\bar{\chi}$ is implied. In the present study, we used Lorentzian line-shape functions in all of our CD spectra simulations to give

(9) (a) Albertsson, J. *Acta Chem. Scand.* **1968**, *22*, 1563. (b) Albertsson, J. *Acta Chem. Scand.* **1970**, *24*, 3527.

(10) Barron, L. D. *Molecular Light Scattering and Optical Activity*; Cambridge University Press: Cambridge, England, 1982.

(11) Mason, S. F. *Molecular Optical Activity and the Chiral Discriminations*; Cambridge University Press: Cambridge, England, 1982.

$$\rho_t(\bar{\nu}) = (\Delta_t/\pi)[(\bar{\nu} - \bar{\nu}_t)^2 + \Delta_t^2]^{-1} \quad (6)$$

where Δ_t denotes the line half-width at half-height for a transition (t) located at $\bar{\nu}_t$. Furthermore, we used a *constant* value of 1.71 for $\bar{\chi}$ over the entire 15 000–27 000-cm^{-1} spectral region of interest, which conforms with our use of $n_\alpha = 1.77$ in the work presented in ref 2.

Finally, we introduce *absorption dissymmetry factors*, which are often used to characterize the chiroptical activity of electronic transitions. These quantities are dimensionless and they are defined by

$$g_{abs}(\bar{\nu}) = \frac{\Delta\epsilon(\bar{\nu})}{\epsilon(\bar{\nu})} \quad (7)$$

where $\epsilon(\bar{\nu}) = [\epsilon_L(\bar{\nu}) + \epsilon_R(\bar{\nu})]/2$. The CD ($\Delta\epsilon$) and absorption ($\epsilon$) lines associated with a purely electronic transition have identical line shapes, and g_{abs} has a constant value across the transition line width. For the transitions (A → B) observed in our axial CD/absorption spectra of HoODA, the absorption dissymmetry factors are given by

$$g_{abs}(A \rightarrow B) = \frac{4\bar{\chi}R_{AB}(\alpha)}{3S_{AB}(\alpha)} \quad (8)$$

where $R_{AB}(\alpha)$ is the axial rotatory strength (as defined in eqs 2–4 of the present paper), and $S_{AB}(\alpha)$ is the axial absorption line strength defined by eqs 4 and 6 of ref 1. Calculated and empirically determined values of $S_{AB}(\alpha)$ are given in refs 1 and 2, and those absorption line strengths may be combined with rotatory strength data to compute absorption dissymmetry factors according to eq 8. Alternatively, g_{abs} values may be determined directly from the $\Delta\epsilon/\epsilon$ ratios observed for CD/absorption lines.

Results

Calculated and experimentally determined rotatory strengths and dissymmetry factors are shown in Table I for transitions originating from the *ground* crystal-field level of the $^5I_8$ multiplet manifold. The calculated rotatory strengths are from evaluations of eq 4 based on the A_{tp}^{λ} parameter values listed under Set (1) in Table I of ref 2. The crystal-field state vectors used in these calculations were obtained as eigenvectors of the parametrized model Hamiltonian described in ref 1. The calculated dissymmetry factors are based on rotatory strengths calculated in the present study and on absorption line strengths calculated according to ref 2. The numbering and labeling of the excited crystal-field levels listed in Table I are identical to those used in our previous work on HoODA.[1,2]

All of the experimentally determined rotatory strengths and dissymmetry factors listed in Table I are based on axial CD and absorption measurements carried out on HoODA at 10 K. Only 21 of the CD/absorption lines assigned to transitions from the *ground* crystal-field level of $^5I_8$ were sufficiently well-resolved and intense to permit quantitative determination of rotatory strengths. Rotatory strengths and dissymmetry factors were determined for three CD/absorption lines assigned to transitions originating from the first excited crystal-field level (14 cm^{-1} above ground) of $^5I_8$. These data are given in Table II.

Absorption and CD spectra measured in five different multiplet-to-multiplet transition regions are shown in Figures 1–5. Simulated CD spectra, based on the use of eq 5, are also shown in these figures. The lines in the "stick" spectra shown under the simulated CD spectra give the locations and relative rotatory strengths *calculated* for the CD-active transitions (with rotatory strengths weighted by the appropriate thermal population factors). The line-width parameters (Δ_t) used in the spectra simulations are given in the figure captions.

In our previous optical absorption studies of HoODA,[1,2] we found that many of the crystal-field levels of E symmetry (in the D_3 point group) exhibit small splittings (≤4 cm^{-1}) at sample temperatures below ≈20 K. These splittings are also apparent in the low-temperature CD spectra measured in the present study. The splittings either vanish or are obscured by line-broadening in spectra recorded at temperatures above 20 K. Rotatory strengths for split transitions were determined by integrating CD intensity ($\Delta\epsilon$) over the transition components. However, no attempts were made to model transition splittings in the simulated spectra.

All of the features observed in the absorption and CD spectra of Figures 1–5 can be assigned to transitions originating from

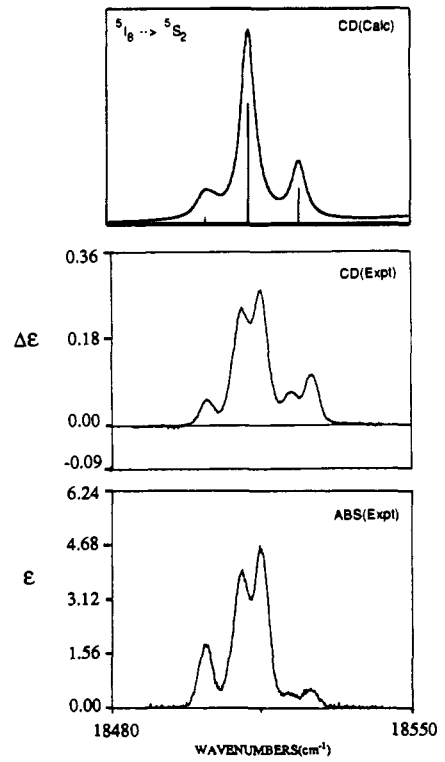

Figure 1. Simulated CD and experimental CD and absorption spectra for the $^5I_8 \rightarrow {}^5S_2$ transition region of HoODA at 10 K. Simulated CD spectra were calculated using the line-width parameter, $\Delta_t = 2$ cm^{-1}.

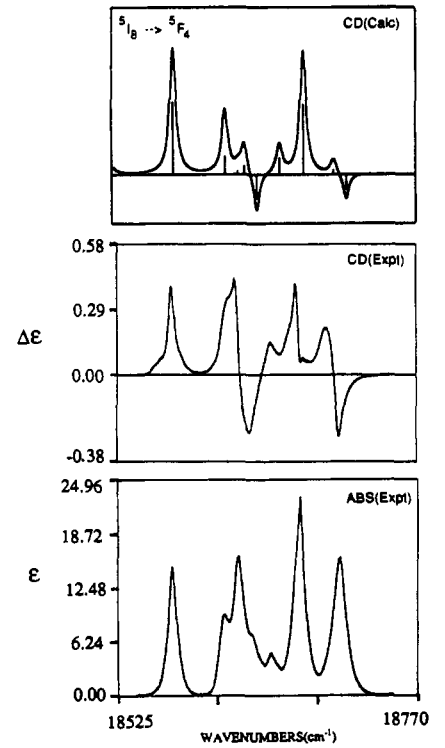

Figure 2. Simulated CD and experimental CD and absorption spectra for the $^5I_8 \rightarrow {}^5F_4$ transition region of HoODA at 10 K. Simulated CD spectra were calculated using the line-width parameter, $\Delta_t = 3$ cm^{-1}.

either the ground crystal-field level (E symmetry) *or* the first excited crystal-field level (A_1 symmetry) of the $^5I_8$ ground multiplet manifold if E-level splittings are taken into account. These assignments are shown explicitly in the axial absorption spectra presented in ref 2. The ground E($^5I_8$) level is split by ≈4 cm^{-1}, and the first excited A_1 ($^5I_8$) level is located 14 cm^{-1} above the centroid of the split ground level. At 10 K, the fractional populations of these levels should be $X(10\ K) = 0.60\ (E_-), 0.34\ (E_+)$,

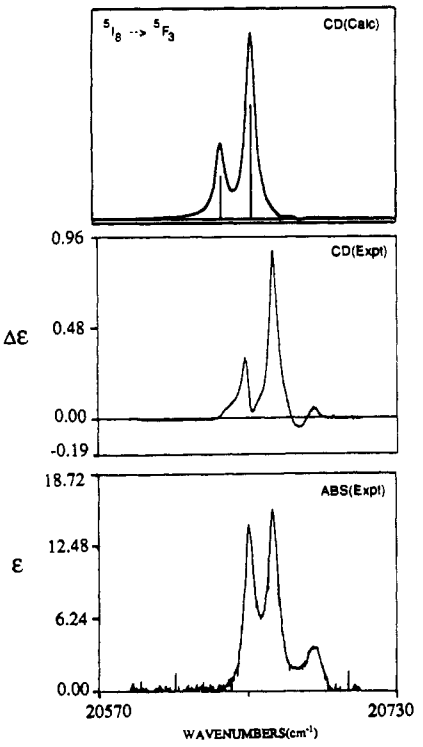

Figure 3. Simulated CD and experimental CD and absorption spectra for the $^5I_8 \rightarrow {}^5F_3$ transition region of HoODA at 10 K. Simulated CD spectra were calculated using the line-width parameter, $\Delta_t = 3$ cm^{-1}.

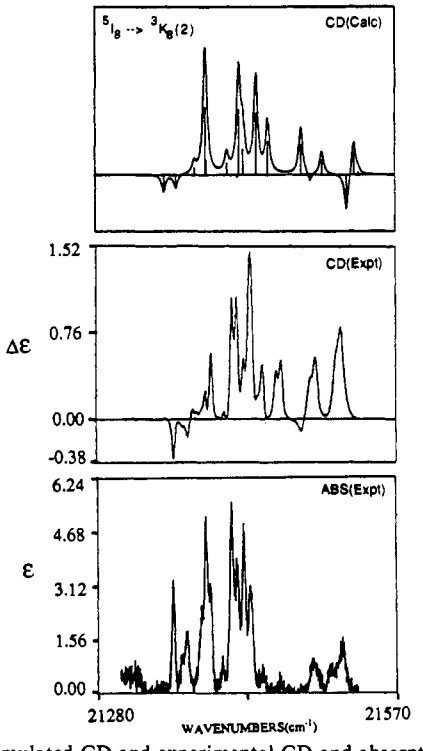

Figure 4. Simulated CD and experimental CD and absorption spectra for the $^5I_8 \rightarrow {}^3K_8$ transition region of HoODA at 10 K. Simulated CD spectra were calculated using the line-width parameter, $\Delta_t = 2$ cm^{-1}.

and 0.06 (A_1), where E_- and E_+ denote the lower and upper components of the split E level. Comparisons of our calculated and experimental spectra suggest that local heating effects produce internal crystal temperatures that are 5–10 °C higher than the measured temperature of 10 K (at the crystal surface). This is indicated by the larger-than-predicted intensity ratios observed for $A_1 \rightarrow \Gamma$ versus $E \rightarrow \Gamma$ transitions. Evidence for local heating effects was also found in our previous optical studies of HoODA.[1,2,12]

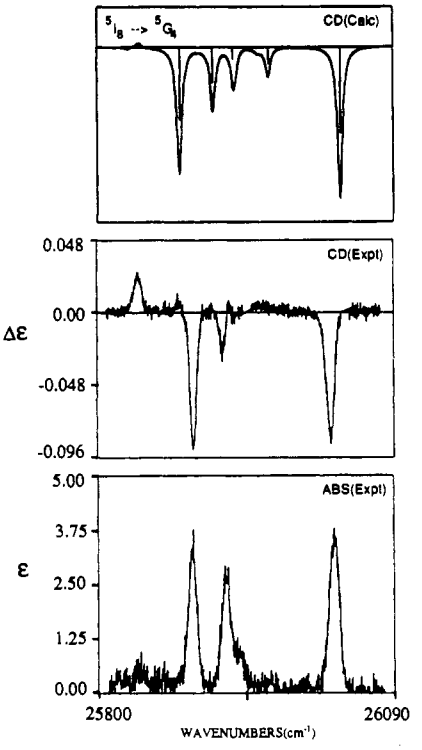

Figure 5. Simulated CD and experimental CD and absorption spectra for the $^5I_8 \rightarrow {}^5G_4$ transition region of HoODA at 10 K. Simulated CD spectra were calculated using the line-width parameter, $\Delta_t = 3$ cm^{-1}.

Only our low-temperature CD/absorption results proved useful for quantitative analysis. At higher temperatures, transitions from additional crystal-field levels of $^5I_8$ begin to contribute and the spectra become congested with overlapping lines and poorly resolved features. The third and fourth crystal-field levels of $^5I_8$ are located at 63 cm^{-1} (an E level) and ≈100 cm^{-1} (an A_2 level), and four additional levels are predicted at energies less than 300 cm^{-1}.[1]

Discussion

Among the multiplet-to-multiplet transition regions examined in this study, the largest absorption dissymmetry factors $|\Delta\epsilon/\epsilon|$ are calculated and observed within the $^5I_8 \rightarrow {}^3K_8(2)$ and $^5I_8 \rightarrow {}^3K_7(2)$ transition manifolds. The transitions within these manifolds have strong $\Delta J = 0$ *or* -1 character, and many are predicted to occur via a predominantly magnetic dipole mechanism.[2] One of the transitions within $^5I_8 \rightarrow {}^3K_8(2)$, level 1(E) to level 75(A_2), exhibits nearly perfect circular polarization, $g_{abs} \approx 2$.

Many CD lines (or features) observed within the $^5I_8 \rightarrow {}^5F_5$, $^5S_2$, $^5F_4$, $^5F_3$, $^5F_2$, $^5G_6$, $^5G_5$, and $^5G_4$ transition regions have intensities ($\Delta\epsilon$) that are comparable to (or greater than) those observed in the $^5I_8 \rightarrow {}^3K_8(2)$ and $^3K_7(2)$ regions. However, the $|\Delta\epsilon/\epsilon|$ ratios are generally much smaller. Transitions in these regions are predominantly electric dipole in character,[2] and they acquire magnetic dipole character only via crystal-field-induced J-multiplet mixing. For predominantly electric dipole transitions, eq 8 may be approximated according to

$$g_{abs} \approx \frac{4\bar{\chi}R_{AB}(\alpha)}{3\chi D^{(e)}_{AB}(\alpha)} \tag{9}$$

where $D^{(e)}_{AB}(\alpha)$ is an axial electric-dipole strength (defined according to eq 11 of ref 5) and $\chi \approx (n_\alpha^2 + 2)^2/9n_\alpha$. The magnitude of this dissymmetry factor is given by

$$|g_{abs}| \approx \frac{4\bar{\chi}|R_{AB}(\alpha)|}{3\chi D^{(e)}_{AB}(\alpha)} = \left(\frac{4\bar{\chi}}{\chi}\right)\frac{|m_{AB,q}|}{|\mu_{AB,q}|} \tag{10}$$

(12) Small differences between the absorption spectra reported here and in ref 2 reflect small differences in the "effective" temperatures of the crystal samples.

Table I. Calculated and Experimentally Determined Rotatory Strengths and Dissymmetry Factors for Transitions Originating from the $E(^5I_8)$ *Ground* Crystal-Field Level

excited level[a]				$R/10^{-44}$ esu^2 cm^2		$g_{abs}/10^{-2}$		excited level[a]				$R/10^{-44}$ esu^2 cm^2		$g_{abs}/10^{-2}$	
no.	multiplet[b]	Γ^c	energy/cm^{-1} [d]	calcd[e]	exptl[f]	calcd[g]	exptl[g]	no.	multiplet[b]	Γ^c	energy/cm^{-1} [d]	calcd[e]	exptl[f]	calcd[g]	exptl[g]
44	$^5F_5$	A_2	15524	17.7	n.d.	13.9	n.d.	79	$^5G_6$	A_1	22100	16.8	n.d.	0.23	n.d.
45		E	15532	22.7	n.d.	43.4	n.d.	80		E	22127	0.94	n.d.	1.2	n.d.
46		A_1	15536	−34.9	n.d.	3.4	n.d.	81		A_2	22156	46.4	n.d.	1.7	n.d.
47		E	15555	298	n.d.	10.3	n.d.	82		A_1	22165	113	n.d.	6.7	n.d.
48		E	(15630)	111	n.d.	12.7	n.d.	83		E	22190	142	n.d.	5.5	n.d.
49		E	(15634)	16.7	n.d.	0.63	n.d.	84		E	22296	22.0	n.d.	0.35	n.d.
50		A_2	15636	−29.4	−55.7	−5.8	−9.9	85		A_2	(22308)	15.2	n.d.	14.9	n.d.
51	$^5S_2$	A_1	(18504)	2.72	n.d.	7.0	n.d.	86		A_1	(22319)	58.5	n.d.	6.0	n.d.
52		E	18513	54.9	29.1	11.2	6.2	87		E	22335	20.2	n.d.	0.59	n.d.
53		E	18525	16.2	12.9	43.0	18.8	88	$^5F_1$	A_2	22397	−2.89	n.d.	2.0	n.d.
54	$^5F_4$	A_1	18573	248	82.1	7.8	2.6	89		E	22409	−0.22	n.d.	4.0	n.d.
55		E	18624	13.3	n.d.	13.8	n.d.	90	$^5G_5$	E	23974	−183	n.d.	−4.7	n.d.
56		E	18636	−80.7	n.d.	−24.3	n.d.	91		E	24008	0.44	n.d.	0.062	n.d.
57		A_1	18651	57.0	18.7	5.8	2.8	92		A_2	24010	−6.28	n.d.	−5.2	n.d.
58		A_2	18673	241	n.d.	5.6	n.d.	93		A_1	(24052)	−10.1	n.d.	−14.9	n.d.
59		E	18705	−51.6	−34.7	−2.6	−1.7	94		E	24083	4.53	n.d.	0.44	n.d.
60	$^5F_3$	A_2	20650	125	53.4	4.3	2.1	95		A_2	24096	−0.005	n.d.	183	n.d.
61		A_1	20663	332	145	10.3	5.6	96		E	24114	−0.85	n.d.	10.9	n.d.
62		E	20688	−5.67	8.40	−0.90	1.3	97	$^5G_4$	E	25843	0.34	n.d.	10.6	n.d.
63		E	20740	0.42	n.d.	1.4	n.d.	98		A_2	25898	−8.77	−5.20	−4.4	−2.6
64		A_2	20672	15.3	n.d.	19.2	n.d.	99		A_1	(25915)	−4.34	n.d.	−10.9	n.d.
65	$^5F_2$	A_1	21124	47.7	n.d.	6.8	n.d.	100		E	25941	0.073	n.d.	0.080	n.d.
66		E	21141	83.0	94.2	22.8	29	101		E	25968	−2.05	n.d.	−5.1	n.d.
67		E	21185	−3.68	6.26	−7.3	9.3	102		A_1	26032	−10.5	−10.1	−6.0	−2.2
68	$^3K_8(2)$	E	21371	−21.3	−14.4	−13.2	−8.9	103	$^3K_7(2)$	E	26193	0.53	n.d.	1.8	n.d.
69		A_2	21388	167	10.5	44.3	4.7	104		A_2	(26207)	−0.64	n.d.	−0.30	n.d.
70		E	21394	36.4	26.7	19.9	18.3	105		A_1	(26208)	−6.29	n.d.	−5.8	n.d.
71		A_1	(21417)	−6.07	n.d.	−9.0	n.d.	106		E	(26210)	14.5	n.d.	26.9	n.d.
72		E	21419	160	n.d.	59.7	n.d.	107		E	26213	−3.61	n.d.	−39.6	n.d.
73		A_1	21426	62.5	n.d.	38.2	n.d.	108		A_2	(26223)	12.0	n.d.	18.6	n.d.
74		E	21444	35.5	81.3	95.0	167	109		E	26231	13.3	n.d.	91.2	n.d.
75		A_2	21462	63.1	64.9	199	199	110		A_1	(26246)	11.9	n.d.	174	n.d.
76		E	21494	70.8	59.1	67.3	60.7	111		E	26242	7.23	n.d.	31.3	n.d.
77		A_1	21518	53.8	125	39.2	76.6	112		A_2	26255	53.9	66.1	194	34.4
78		E	(21523)	6.53	n.d.	69.0	n.d.								

[a] The excited crystal-field levels are identified according to the numbering and labeling scheme used in Table II of ref 1. [b] Identifies the *principal SLJ* parentage of the crystal-field states. [c] Irreducible representation label in the D_3 point group. [d] Energies shown in parentheses are from calculations.[1] All other energies are from experimental observation. [e] Calculated according to eq 4 (see text). [f] Evaluated according to eq 2 (see text) using CD/absorption data measured at 10 K. Uncertainties in the reported values are approximately ±10%. n.d. ≡ *not determined*. [g] See eqs 7 and 8 of the text for definitions of the absorption dissymmetry factor g_{abs}.

where $m_{AB,q}$ and $\mu_{AB,q}$ denote $q = \pm 1$ polarized components of the magnetic and electric dipole transition moments. For HoODA, $\bar{\chi}/\chi \approx 1.03$ (assuming $n_\alpha \approx 1.77$, vide supra), and

$$\frac{|m_{AB,q}|}{|\mu_{AB,q}|} \approx 0.24|g_{abs}| \qquad (11)$$

Among the transitions listed in Tables I and II, the great majority with $|\Delta J| > 1$ parentage are either observed or calculated to have $|g_{abs}|$ values less than 0.15, which from eq 11 imply $|m|/|\mu|$ ratios smaller than 0.04. The most prominent exceptions are found in the $^5I_8 \rightarrow {}^5S_2$ and $^5I_8 \rightarrow {}^5F_2$ transition regions where $0.15 < |g_{abs}| < 0.30$ for several transitions. The baricenter of the $^5F_2$ multiplet manifold is located less than 300 cm^{-1} below the baricenter of $^3K_8(2)$,[1] and our calculations show mixing between $^5F_2$ and $^3K_8$ levels. This mixing is small, but it is sufficient to introduce ca. 5% magnetic dipole character into one of the $E(^5I_8) \rightarrow E(^5F_2)$ transitions. The origins of $^5I_8 \rightarrow {}^5S_2$ magnetic dipole character are less readily apparent from a crystal-field eigenvector analysis because the eigenvectors show essentially no mixing between $^5S_2$ and $^3K_8$ (or $^3K_7$) levels.

The calculated and experimentally observed CD spectra shown in Figures 1–5 are in reasonably good agreement, particularly when one takes into account the small disparities between calculated and observed transition frequencies, the neglect of E-level splittings in the simulated spectra, and the possibility that the experimental spectra reflect a sample temperature 5–10 °C higher than 10 K. The presence of E-level splitting is most apparent in the $^5I_8 \rightarrow {}^5S_2$ absorption and CD spectra shown in Figure 1. The peaks at 18527 and 18523 cm^{-1} are assigned to split components of one $E(^5I_8) \rightarrow E(^5S_2)$ transition, the peaks at 18515 and 18510 cm^{-1} are assigned to split components of another $E(^5I_8) \rightarrow E(^5S_2)$ transition, and the band centered at ≈18499 cm^{-1} is assigned to an $A_1(^5I_8) \rightarrow E(^5S_2)$ transition. The intensity asymmetry observed within each pair of split E → E transitions reflects differential populations of the two levels split out of $E(^5I_8)$.

Comparisons between the calculated and experimental data given in Tables I and II indicate mixed success in our calculations of transition rotatory strengths and dissymmetry factors. Overall, the agreement between calculated and experimental results is better than might be expected for a system as complicated as HoODA, with its complex $4f^{10}$ electronic state structure and closely spaced *J*-multiplet manifolds. However, the agreement is poorer than that achieved in our previous analyses of SmODA and EuODA chiroptical properties.[5,6] Correct signs are calculated for all but two of the 24 empirically characterized transition rotatory strengths, and for the majority of transitions, the magnitudes of the calculated and empirical rotatory strengths agree to within a factor of 2. However, in several cases there is substantial disagreement between the calculated and empirical rotatory strengths.

The rotatory strength calculations carried out in this study were based on the same intensity model employed in our earlier analysis of 4f–4f absorption line strengths in HoODA optical spectra.[2] Identical intensity parameters and crystal-field state vectors were used to calculate transition rotatory strengths and dipole (line) strengths. Agreement between calculation and experiment is significantly better for dipole strengths than for rotatory strengths.

Table II. Calculated and Experimentally Determined Rotatory Strengths and Dissymmetry Factors for Transitions Originating from the First Excited Crystal-Field Level, A_1, of $^5I_8$

excited level[a]				$R/10^{-44}$ esu^2 cm^2		$g_{abs}/10^{-2}$	
no.	multiplet[b]	Γ[c]	energy/cm^{-1}[d]	calcd[e]	exptl[f]	calcd[g]	exptl[g]
51	$^5S_2$	A_1	(18 495)	f			
52		E	18 499	16.3	15.8	8.7	2.8
53		E	18 511	1.54	n.d.	95.8	n.d.
65	$^5F_2$	A_1	(21 115)	f			
66		E	21 127	50.7	n.d.	8.6	n.d.
67		E	21 171	83.6	125	13.9	17.3
68	$^3K_8(2)$	E	21 357	−73.1	−101	−19.0	−19.5
69		A_2	(21 379)	f			
70		E	21 380	46.2	n.d.	125	n.d.
71		A_1	(21 408)	f			
72		E	21 405	78.3	n.d.	57.6	n.d.
73		A_1	(21 414)	f			
74		E	21 430	408	n.d.	105	46.9
75		A_2	(21 464)	f			
76		E	21 480	−38.2	n.d.	−147	n.d.
77		A_1	(21 511)	f			
78		E	(21 514)	−156	n.d.	113	n.d.

[a] The excited crystal-field levels are identified according to the numbering and labeling scheme used in Table II of ref 1. [b] Identifies the *principal SLJ* parentage of the crystal-field states. [c] Irreducible representation label in the D_3 point group. [d] Energies shown in parentheses are from calculations.[1] All other energies are from experimental observation. [e] Calculated according to eq 4 (see text). f ≡ forbidden (by symmetry). [f] Evaluated according to eq 2 (see text) using CD/absorption data measured at 10 K. Uncertainties in the reported values are approximately ±10%. n.d. ≡ *not determined*. [g] See eqs 7 and 8 of the text for definitions of the absorption dissymmetry factor g_{abs}.

This is most likely attributable to the much greater sensitivity of rotatory strength calculations to the detailed $SLJM_J$ compositions of state vectors and to the relative signs and magnitudes of the intensity model parameters (the A^λ_{tp} parameters in eq 4).[4-6] The low-temperature absorption and CD spectra of HoODA give clear evidence for small deviations from the D_3 crystal-field symmetry assumed in our energy-level and intensity models.[1,2] It is possible that these deviations (reflected in the small E-level splittings) have special consequences for rotatory strengths, but are inconsequential contributors to unpolarized (*axial*) and linearly polarized (*orthoaxial*) absorption line strengths. There is some evidence that $Na_3[Ln(ODA)_3]\cdot 2NaClO_4\cdot 6H_2O$ systems undergo a low-temperature phase transition in which the crystal space group changes from *R*32 to *P*321, and the lanthanide site symmetry is reduced from D_3 to C_2 (due to movement of the Na^+ ions off 3-fold axes).[13-15]

Additional rotatory strength data would permit refinements of the energy-level and intensity models for HoODA, but those data are very difficult to obtain from the congested CD spectra. The models employed in the present study have obvious shortcomings, but they provide a useful (and generally satisfactory) basis for qualitative and semiquantitative interpretation of the experimental results. Intensities of optical transitions between Stark levels in structurally complex lanthanide systems are notoriously difficult to model and rationalize,[3,16-23] and the chiroptical properties of these transitions make yet additional demands on intensity models and theory.[4-6,14] Rotatory strengths depend (to lowest order) on scalar products of *electric* and *magnetic* dipole transition vectors, so *both* of these quantities must be accurately characterized (or calculated) in chiroptical intensity models. In the calculations reported in this paper, magnetic dipole transition vectors are calculated directly from the eigenvectors of a model Hamiltonian parametrized to yield optimal fits between calculated and empirical energy-level data.[1] These same eigenvectors are also used in calculations of electric dipole transition vectors, *along* with a set of intensity parameters (A^λ_{tp}) derived from fits of calculated-to-empirical absorption line-strength data.[2] The calculated rotatory strengths are particularly sensitive to the relative signs and magnitudes of the A^λ_{tp} parameters, but no attempts were made to fit calculated-to-empirical rotatory strength data by varying the A^λ_{tp} parameters away from the values reported in ref 2. The empirical data set of 24 rotatory strengths is too small to support a meaningful parametric analysis (in which all 12 of the A^λ_{tp} parameters are freely varied).

Acknowledgment. This work was supported by the National Science Foundation (NSF Grant CHE-88-20180). We also gratefully acknowledge considerable help from Dr. Michael F. Reid in carrying out the calculations reported in this paper.

(13) Schwartz, R. W.; Banerjee, A. K.; Chowdhury, M.; Kuroda, R. *J. Chem. Soc., Faraday Trans. 2* **1981**, *77*, 557.
(14) Vala, M.; Szczepanski, J.; Banerjee, A. K.; Chowdhury, M. *Chem. Phys.* **1989**, *134*, 149.
(15) Dasgupta, S.; Saha, M.; Ghosh, G. *J. Phys. C* **1986**, *19*, 1771.
(16) Dallara, J. J.; Reid, M. F.; Richardson, F. S. *J. Phys. Chem.* **1984**, *88*, 3587.
(17) May, P. S.; Reid, M. F.; Richardson, F. S. *Mol. Phys.* **1987**, *61*, 1471.
(18) Berry, M. T.; Schwieters, C.; Richardson, F. S. *Chem. Phys.* **1988**, *122*, 105.
(19) May, P. S.; Jayasankar, C. K.; Richardson, F. S. *Chem. Phys.* **1989**, *138*, 139.
(20) Reid, M. F. *J. Chem. Phys.* **1987**, *87*, 6388.
(21) Mason, S. F. *J. Less-Common Met.* **1983**, *93*, 45.
(22) Stewart, B. *Mol. Phys.* **1983**, *50*, 161.
(23) Newman, D. J.; Balasubramanian, G. *J. Phys. C* **1975**, *8*, 37.